MDPI

Article

Modeling the Land Surface Phenological Responses of Dominant Miombo Tree Species to Climate Variability in Western Tanzania

Siwa E. Nkya [1,2,*], Deo D. Shirima [3,4], Robert N. Masolele [5], Henrik Hedenas [6] and August B. Temu [7]

[1] Regional Research School in Forest Sciences (REFOREST), College of Forestry, Wildlife, and Tourism, Sokoine University of Agriculture, Morogoro P.O. Box 3009, Tanzania
[2] Tanzania Forestry Research Institute, Morogoro P.O. Box 1854, Tanzania
[3] Department of Ecosystems and Conservation, College of Forestry, Wildlife, and Tourism, Sokoine University of Agriculture, Morogoro P.O. Box 3010, Tanzania; dshirima@sua.ac.tz
[4] National Carbon Monitoring Centre, Sokoine University of Agriculture, Morogoro P.O. Box 3009, Tanzania
[5] Laboratory of Geo-Information Science and Remote Sensing, Environmental Sciences Group, Wageningen University & Research, Postbus 47, 6700AA Wageningen, The Netherlands; robert.masolele@wur.nl
[6] Department of Forest Resource Management, Swedish University of Agricultural Sciences, Skogsmarksgränd, SE-901 83 Umeå, Sweden; henrik.hedenas@slu.se
[7] College of Forestry, Wildlife, and Tourism, Sokoine University of Agriculture, Morogoro P.O. Box 3009, Tanzania; killemery@gmail.com
* Correspondence: siwa.nkya@tafori.or.tz; Tel.: +255-(0)-713-414589

Abstract: Species-level phenology models are essential for predicting shifts in tree species under climate change. This study quantified phenological differences among dominant miombo tree species and modeled seasonal variability using climate variables. We used TIMESAT version 3.3 software and the Savitzky–Golay filter to derive phenology metrics from bi-monthly PlanetScope Normalized Difference Vegetation Index (NDVI) data from 2017 to 2024. A repeated measures Analysis of Variance (ANOVA) assessed differences in phenology metrics between species, while a regression analysis modeled the Start of Season (SOS) and End of Season (EOS). The results show significant seasonal and species-level variations in phenology. *Brachystegia spiciformis* differed from other species in EOS, Length of Season (LOS), base value, and peak value. Surface solar radiation and skin temperature one month before SOS were key predictors of SOS, with an adjusted R-squared of 0.90 and a Root Mean Square Error (RMSE) of 13.47 for *Brachystegia spiciformis*. SOS also strongly predicted EOS, with an adjusted R-squared of 1 and an RMSE of 3.01 for *Brachystegia spiciformis*, indicating a shift in the growth cycle of tree species due to seasonal variability. These models provide valuable insights into potential phenological shifts in miombo species due to climate change.

1. Introduction

Miombo woodlands thrive in tropical Africa and are dominated by the *Brachystegia*, *Julbernadia*, and/or *Isorberlinia* genera [1]. Wet miombo woodlands receive annual rainfall ranging from 800 to 1500 mm and a dry period lasting from 3 to 5 months, whereas dry miombo woodlands receive annual rainfall ranging from 500 to 1000 mm with a dry period lasting from 5 to 8 months [2,3]. The woodlands cover 2 million km^2 across Angola, Zimbabwe, Zambia, Malawi, Mozambique, Tanzania, and the Democratic Republic of Congo [4]. In these countries, miombo woodlands play a major role in livelihoods by providing household energy, timber, and food such as mushrooms, fruits, and honey [5–8].

The increasing demand for forest products and the expansion of cropland due to population growth result in woodland loss [7–9], threatening the existence of miombo tree species [10]. Another threat to miombo tree species are rising temperatures, which are projected to reduce 5% of the already degraded miombo woodland cover in Tanzania by

2085 [11]. Miombo woodlands in wetter areas are expected to decline by up to 42% by 2070, while those in drier areas may increase by 23% over the same period in Sub-Saharan Africa [12]. This shift suggests that climate change could impact the canopy cover, thereby causing a significant threat to the ecosystem and livelihoods of communities depending on the woodlands.

Empirical information on the response of tree species to climate variability and change is essential for understanding the effects of climate change on miombo woodland development. One measure that could provide insights into the response of tree species to climate is phenology, which is strongly influenced by climate [13,14]. Phenology is the study of the timing of recurrent biological events, how these events are influenced by climate and human activities, and how they relate among species. In vegetation, phenological events include, among others, leaf budburst, leaf shedding, first flower, last flower, and first ripe fruit. These events are specific traits of each plant species, and the combined effects of all species characterize and maintain an ecosystem [15,16].

Space-borne optical sensors are primarily applied to track Land Surface Phenology (LSP) in miombo woodlands [17]. Remote sensing is a cost-effective approach, allowing for frequent monitoring across vast and remote areas, making it more practical than ground-based methods. Coarse-resolution remote sensors are commonly used, limiting phenology monitoring efforts to the vegetation level. Monitoring LSP at this scale has shown that temperature better explains variations in miombo vegetation phenology than precipitation [18]. Additionally, photoperiods are identified as reliable predictors of the start of the season, while both temperature and photoperiod were reliable predictors of the end of the season for Southern African savanna trees [19]. These factors contribute to the observed pre-rain green-up and post-rain dormancy onset in savannas and woodlands, including miombo woodlands [20,21].

Information on the phenological dynamics of miombo tree species and their interactions with climate is limited. This is due to the mixed pixel effect, where the pixel value of course–resolution satellite images contains reflectance from multiple species and vegetation types. Species-specific phenology information is needed, as phenology is a species-specific trait [22].

With advances in remote sensing technology, particularly sensors with very high spatial resolution and global daily revisit capabilities, this study aimed to develop a climate-driven phenology model for dominant tree species in western Tanzania using high-resolution sensors. Such models are essential for predicting shifts in species ranges in response to environmental changes. The specific objectives of the study were:

(i)   To calculate average phenological metrics: Start of the Season (SOS), End of the Season (EOS), Length of the Season (LOS), Maximum Normalized Difference Vegetation Index (MaxNDVI), and NDVI at Maximum Time (NDVItmax) for the dominant tree species;

(ii)   To quantify the differences in phenological metrics among the dominant tree species;

(iii) To model the effects of climate on the leaf phenological changes in dominant tree species in miombo woodlands.

2. Materials and Methods

2.1. Study Area

The study was conducted on a 9-hectare site within the Tongwe West Forest Reserve in the Tanganyika District of the Katavi Region (Figure 1). The site is located at 30°29′13″E longitude and 5°27′41″S latitude, with an elevation of 1492 m above sea level. The average yearly temperature ranges from 15 °C to 25 °C, and the total annual rainfall is 1210 mm. The soil at the site is predominantly ferralic cambisols with moderately deep to deep soils and moderate to high fertility [23]. These climatic and edaphic conditions support the wet miombo woodlands.

Most miombo tree species are deciduous, shedding their leaves during the dry season. Consequently, distinct leafing phenology seasons have been observed, as follows: the warm dry pre-rain season (September), the rainy season (October–April), and the dry

season (May–August). Given the close linkage between climate and phenology, miombo phenology could serve as a valuable bio-indicator of the effects of climate variability and change on miombo woodland species. The dominant miombo tree species at the site are *Brachystegia spiciformis* (Mtundu), *Julbernardia globiflora* (Muva), and *Pterocarpus tinctorius* (Mkurungu), which dominate the woody biomass [24].
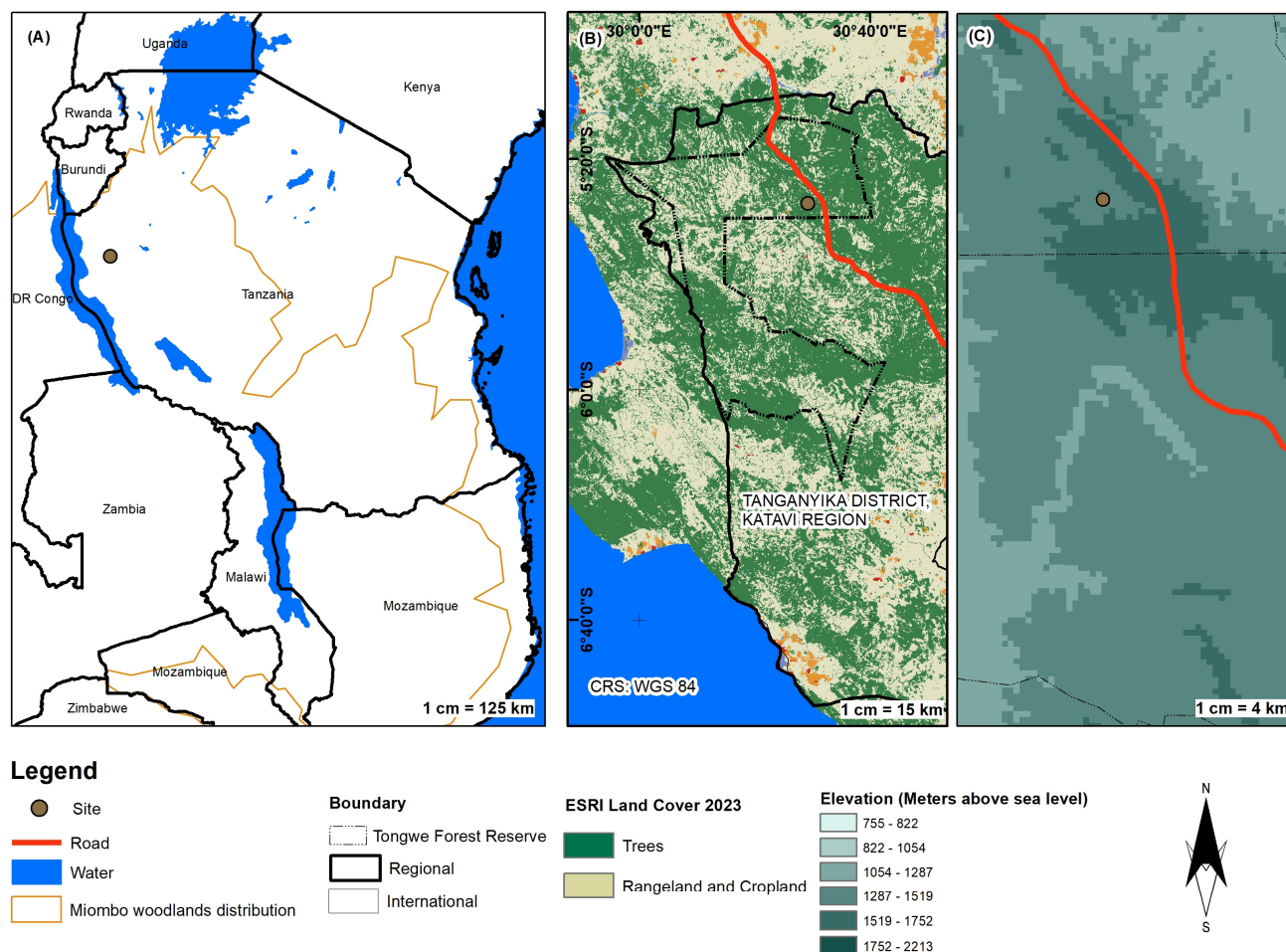

Figure 1. Site location: (**A**) within the miombo woodland distribution, (**B**) in Tongwe Forest Reserve, Tanganyika District, Katavi Region, Tanzania, and (**C**) at elevations measured in meters above sea level.

2.2. Flow Chart

Figure 2 illustrates the type of data collected and the methods used.

2.3. Collection of Data

2.3.1. Tree Crown Data

To obtain the tree crown layer, we selected tree crowns with a minimum area of 9 m² (equivalent to a PlanetScope pixel) that were solitary or part of populations of the same tree species on the ground. The selection was made concurrently by acquiring tree coordinates using differential GPS. After that, we established 16 Ground Control Points (GCPs) on the site for geo-referencing images.

We acquired drone images using the Mavic Air 2S with an RGB sensor on 13 March 2024 at 08:30 a.m. (East Africa Time). The drone flew in an east–west direction at a speed of 15.7 km/h and an altitude of 40 m above ground. The images had 80% forward and 80% side overlap, with a spatial resolution of 1 cm.
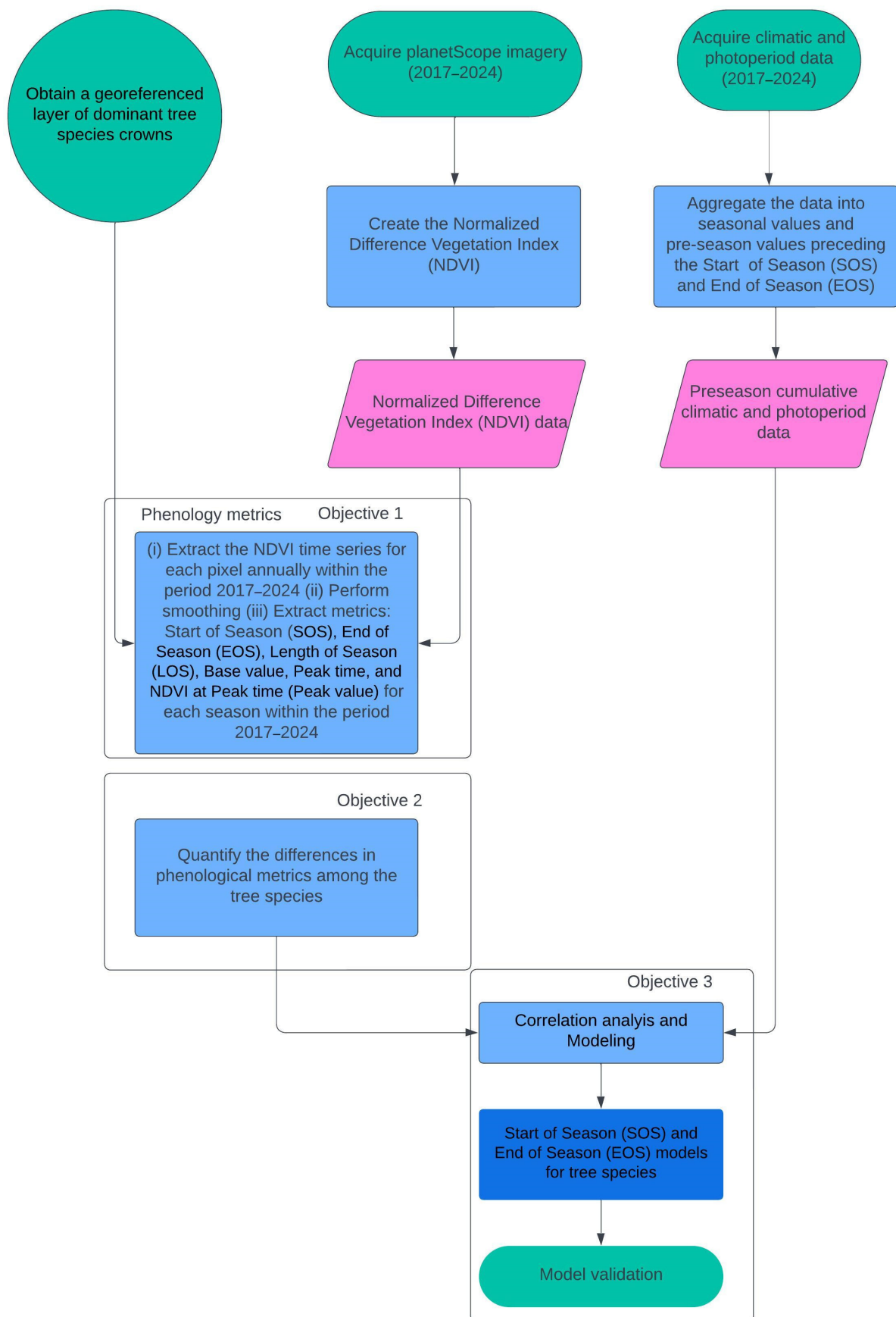
Figure 2. Flow chart of the materials and methods.

Agisoft Metashape Professional software, version 1.5.1, was used to create the orthomosaics, which were geo-referenced using 16 Ground Control Points (GCPs). The coordinates of individual tree crowns were aligned with their corresponding crowns, and the tree species were digitized from the drone orthophoto in ArcMap 10.4.1 software. In total, we digitized 21 crowns for *Brachystegia spiciformis* (*B. spiciformis*), 21 for *Julbernardia globiflora* (*J. globiflora*), 21 for *Pterocarpus tinctorius* (*P. tinctorius*), and 13 for a combined class of other species for this study (Figure 3).
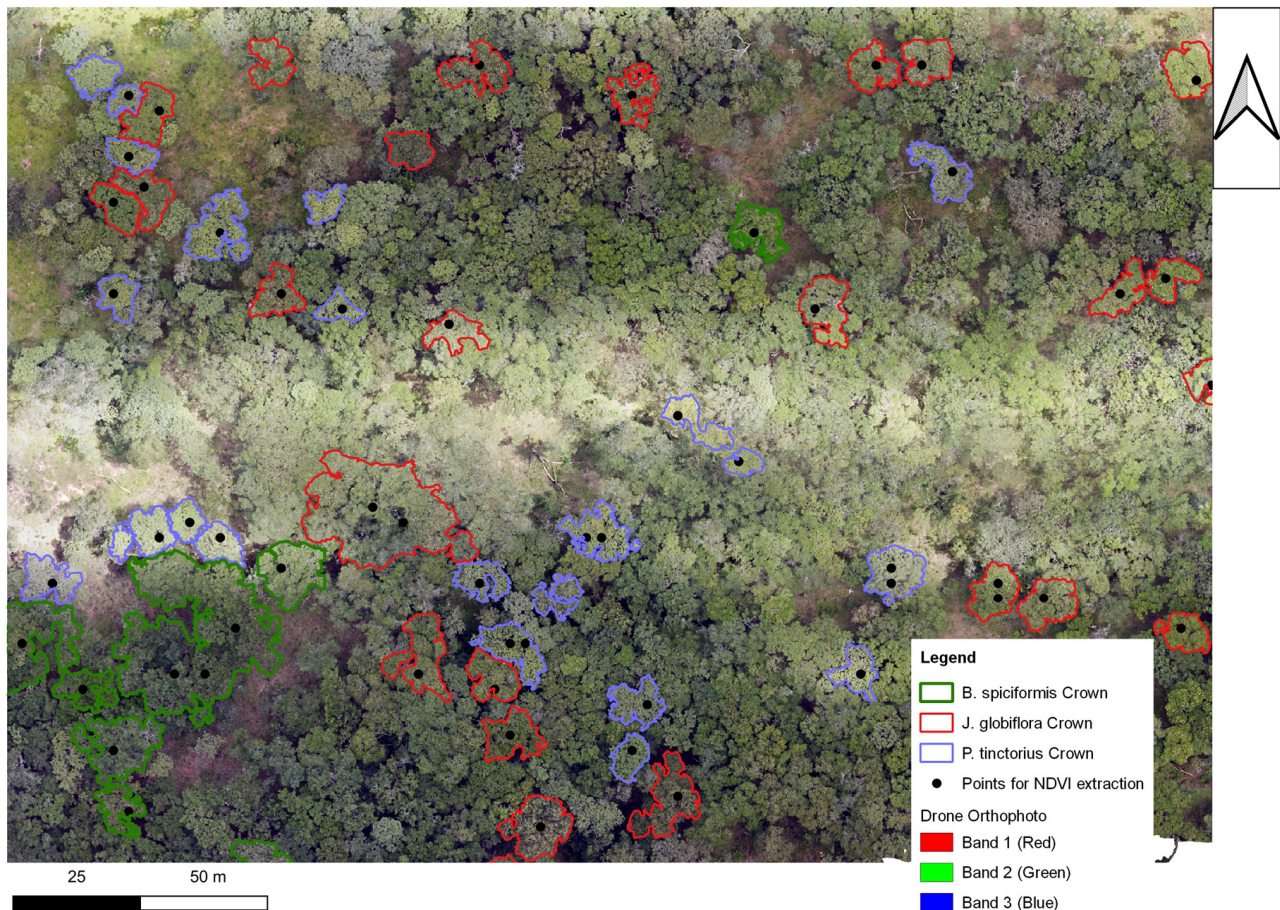

Figure 3. Layer of selected tree species crowns and their points for NDVI extraction, digitized from the drone orthophoto of the site in western Tanzania.

The digitized tree crowns were used to extract 21 pure pixel values from PlanetScope NDVI images for each species group: *Brachystegia spiciformis (B. spiciformis)*, *Julbernardia globiflora (J. globiflora)*, *Pterocarpus tinctorius (P. tinctorius)*, and others.

2.3.2. PlanetScope Images

PlanetScope surface reflectance images with four bands and a spatial resolution of 3 m × 3 m, covering the site, were obtained from Planet Labs under a research license. From 2017 to 2024, we selected two images per month—one for the first half and one for the second half of the month—targeting those with the lowest cloud cover percentage (Appendix B). These surface reflectance data are ideal for analytical applications, and from them, Normalized Difference Vegetation Index (NDVI) layers—a measure of greenness—were created using Formula (1). The NDVI metric was used because of its simplicity and sensitivity to canopy changes [18,21,25]. Additionally, this study focused exclusively on

tree crowns, minimizing interference from soil reflectance, and aimed to observe relative changes in canopy greenness over time.

$$NDVI = \frac{NIR - Red}{NIR + Red} \tag{1}$$

where *NIR* and *Red* are the reflectance values in the near-infrared and red bands, respectively.

2.3.3. Climatic and Photo-Period Data

The most influential variables for the vegetation phenology in Africa were rainfall, temperature, solar radiation, and, most importantly, the photoperiod [19]. Monthly rainfall data in mm were obtained from the Climate Hazards Group InfraRed Precipitation with Station data (CHIRPS) [26]. CHIRPS is a gridded rainfall time series with a spatial resolution of 0.05° (5714.59 m) created from satellite imagery and in situ station data.

The monthly skin temperature and surface solar radiation downwards, obtained from the Copernicus Climate Data Store [27] were used for temperature and solar radiation data, respectively. These data are from the ERA5-Land reanalysis dataset, obtained at a spatial resolution of 0.1° (11,130.66 m). Skin temperature, measured in Kelvin, represents the temperature of the Earth's surface. Surface solar radiation downwards, measured in joules per square meter ($J\,m^{-2}$), is the amount of solar radiation (also known as shortwave radiation) reaching the Earth's surface.

The photoperiod data were the day length data in hours, obtained from the Time and date website [28].

2.4. Methods

2.4.1. Determination of Phenological Metrics

We calculated Land Surface Phenology (LSP) metrics—Start of the Season (SOS, Start t), End of the Season (EOS, End t), Length of the Season (LOS, length), Base Value (Base val.), Peak time (Peak t.), and NDVI at Peak time (Peak value, Peak val.)—from the seasonal NDVI pattern of each point representing tree species crowns in ASCII format using the TIMESAT version 3.3 software (Figure 4) [29–31].

The Savitzky–Golay method was used for fitting seasonal NDVI patterns in TIMESAT (Figure 4). The NDVI data range was from 0.2 to 0.9, and the median filter spike method was applied under common settings. Under class-specific settings, a seasonal parameter of 1 (for one season), an adaptation strength of 2, and a Savitzky–Golay window size of 2 were used. Seasonal amplitude was used to define the start and end of the season, with a value of 0.2 for both. In this case, the Start of the Season (SOS) was defined when NDVI exceeded 20% of the seasonal amplitude, and EOS was defined when NDVI fell below 20% of the seasonal amplitude [21]. Seasonal amplitude (Ampl.) is the difference between the peak value (peak val.) and the base value (base val.).

The LSP metrics were computed for each pixel of the dominant tree species. Repeated measures analysis of variance (ANOVA) was used to assess significant variations in LSP metrics between the tree species.
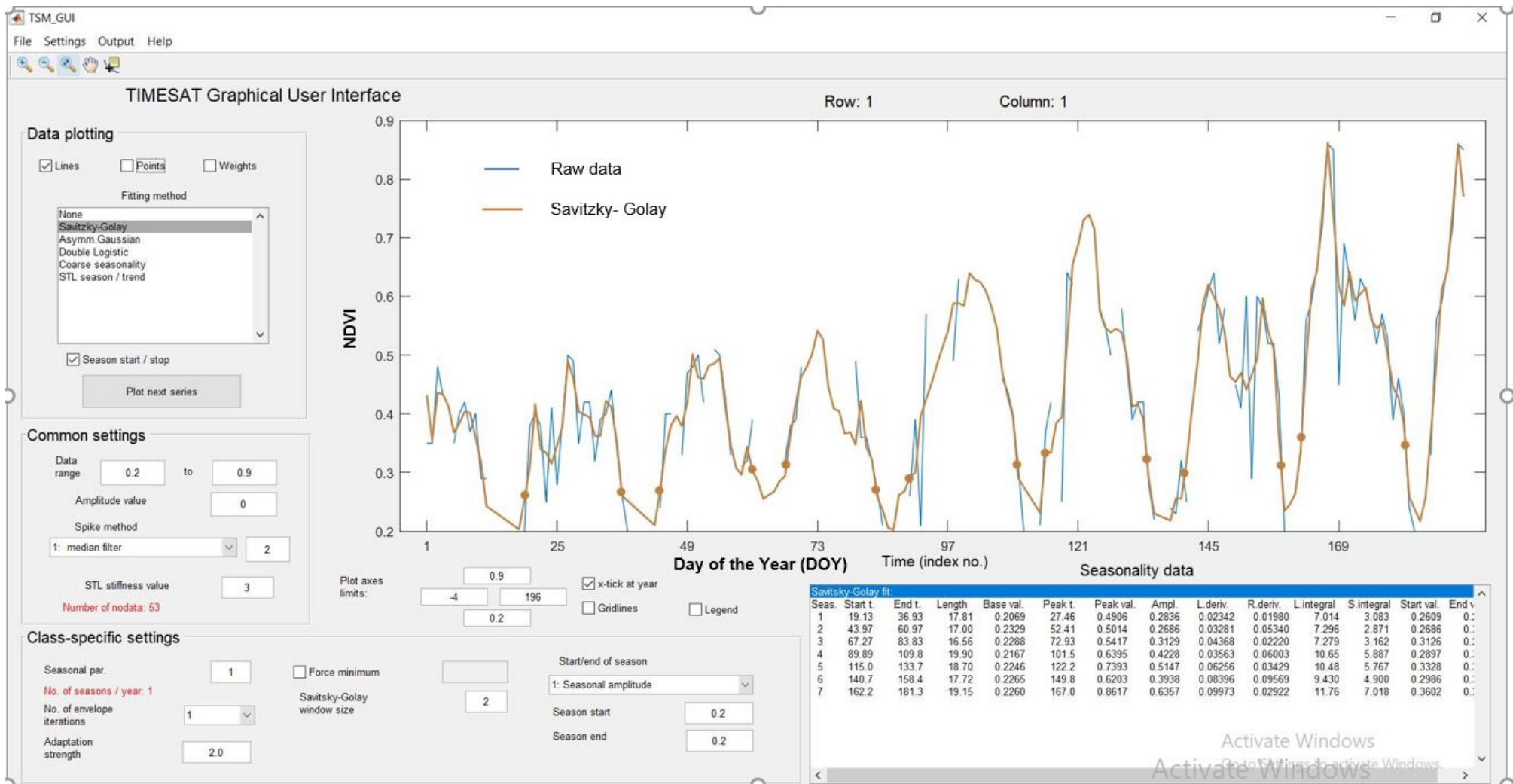
Figure 4. Generation of phenological metrics per season (Seas.) and point (Row) in TIMESAT for this study.

2.4.2. Modeling Phenology Parameters with Climatic Drivers

Before modeling, climatic and photoperiod data aggregated from a zero to three months period preceding the Start of Season (SOS) dates and End of Season (EOS) months for each year were used. The data at zero were termed as seasonal data, while those in the one month, two month, and three month periods before the SOS and EOS date were termed pre-season data.

The spatial climatic data—rainfall, skin temperature, and surface solar radiation—were matched to the tree crown data using the same Coordinate Reference System (CRS). Due to the coarse spatial resolutions of the rainfall, temperature, and solar radiation data, all points representing tree crowns fell within a single pixel (Appendix A). Monthly rainfall, skin temperature, and surface solar radiation values were extracted for each point representing a tree species' crown.

The relationships between the SOS and EOS with seasonal and pre-season cumulative rainfall (mm), cumulative temperature ($^\circ$C), cumulative solar radiation (W/m^2), and cumulative photoperiod (h) for different species were quantified using a correlation analysis and modeled using linear regression. The correlation coefficient was used to assess variable importance and identify the dominant climatic drivers. The models were evaluated using the adjusted R-squared (R^2) metric and the Root Mean Squared Error (RMSE). The RMSE was determined using Equation (2).

$$RMSE = \sqrt[2]{\frac{\sum_{i=1}^{N}(y_i - \hat{y}_i)^2}{N}} \tag{2}$$

where N is the number of observations, y_i is the observed value for the i-th observation, and $\hat{y}$ is the predicted value for the i-th observation.

We used eight points to generate SOS and EOS observations for seven seasons (from 2017 to 2024) to validate the models. This resulted in 56 SOS and 56 EOS observations for both *B. spiciformis* and *J. globiflora*, which were used to validate the SOS and EOS models, respectively.

3. Results

3.1. Differences in the Phenological Metrics for the Dominant Tree Species Across Seasons

We found that the mean SOS for *B. spiciformis* was 90.091 (1 October), *J. globiflora* was 90.026 (1 October), *P. tinctorius* was 90.392 (6 October), and other species were 89.814 (27 September). The mean EOS for *B. spiciformis* was 107.24 (19 June), *J. globiflora* was 108.075 (3 July), *P. tinctorius* was 108.32 (6 July), and for other species was 108.163 (4 July). The mean peak time for *B. spiciformis* was 98.861 (12 February), *J. globiflora* was 98.493 (8 February), *P. tinctorius* was 98.87 (13 February), and for other species was 98.186 (2 February) (Table 1).

The Analysis of Variance (ANOVA) results reveal a statistically significant two-way interaction between species and seasons for all phenological metrics (Table 2). According to the Bonferroni-adjusted p-value (Table 3), the mean SOS differed significantly between *P. tinctorius* and the other species, while the mean EOS showed significant differences between *B. spiciformis* and the rest—*J. globiflora*, *P. tinctorius*, and other species—contributing to the mean LOS of *B. spiciformis* being significantly different from the rest. Additionally, the mean base value for *B. spiciformis* differed significantly from the rest—*J. globiflora*, *P. tinctorius*, and other species. The mean peak time showed significant differences between *B. spiciformis* and other species and between *P. tinctorius* and other species. The mean peak value differed significantly between *B. spiciformis* and the rest—*J. globiflora*, *P. tinctorius*, and other species— as well as between *J. globiflora* and *P. tinctorius*, between *J. globiflora* and other species, and between *P. tinctorius* and other species. Overall, *B. spiciformis* exhibited significant differences in EOS, LOS, base value, and peak value compared to the rest—*J. globiflora*, *P. tinctorius*, and other species.

Table 1. Start of Season (SOS), End of Season (EOS), Length of Season (LOS), base value, peak time, and peak value averaged over eight years (seven seasons) [a].

Species	Start of Season (SOS), DOY		End of Season (EOS), DOY		Length of Season (LOS), Days		Base Value		Peak Time		Peak Value	
	Mean	**sd**	**Mean**	**sd**	**Mean**	**sd**	**Mean**	**sd**	**Mean**	**sd**	**Mean**	**sd**
B. spiciformis	90.091	49.34	107.239	48.99	17.144	2.951	0.255	0.034	98.861	47.058	0.618	0.127
J. globiflora	90.026	48.232	108.075	49.099	18.05	2.405	0.226	0.019	98.493	47.445	0.567	0.136
P. tinctorius	90.392	48.328	108.32	48.851	17.926	2.418	0.227	0.022	98.87	47.359	0.587	0.131
Other	89.814	48.288	108.163	49.125	18.347	2.333	0.226	0.018	98.186	47.162	0.545	0.138

[a] DOY = day of the year, a specific day within a calendar year, sd = standard deviation.

Table 2. Analysis of Variance (ANOVA) results on the difference between phenological metrics across species and seasons [b].

Dependent Variable	Effect	Numerator Degree of Freedom (DFn)	Denominator Degree of Freedom (DFd)	F Value	*p*-Value	*p* < 0.05	Generalized Eta-Squared (ges)
Start of Season (SOS), DOY	Species	2.02	40.31	5.536	0.007	*	0.054
	Season	3.54	70.72	46.682	<0.001	*	0.309
	Species * × Season	5.76	115.16	15.501	<0.001	*	0.297
End of Season (EOS), DOY	Species	1.84	36.79	8.429	0.001	*	0.119
	Season	3.34	66.74	247,077.8	<0.001	*	0.999
	Species × Season	6.11	122.22	4.359	<0.001	*	0.092
Length of Season (LOS), days	Species	2.02	40.31	5.536	0.007	*	0.054
	Season	3.54	70.72	46.682	<0.001	*	0.309
	Species × Season	5.76	115.16	15.501	<0.001	*	0.297
Base value	Species	3	60	24.528	<0.001	*	0.25
	Season	3.15	62.95	7.427	<0.001	*	0.057
	Species × Season	6.5	129.93	8.354	<0.001	*	0.157
Peak time	Species	1.76	35.18	7.902	0.002	*	0.049
	Season	3.35	66.93	166,374.9	<0.001	*	0.999
	Species × Season	5.23	104.59	4.211	0.001	*	0.121
Peak value	Species	2.02	40.46	35.103	<0.001	*	0.427
	Season	2.35	46.97	2658.579	<0.001	*	0.945
	Species × Season	5.43	108.64	17.92	<0.001	*	0.222

[b] DOY = day of the year, a specific day within a calendar year; and "*" indicates significant at *p*-value < 0.05.

Table 3. Pairwise comparison between species in Start of Season (SOS), End of Season (EOS), Length of Season (LOS), base value, peak time, and peak value [c].

Dependent Variable	Group1	Group2	n1	n2	Statistic	df	*p*	*p*.adj	*p*.adj.signif
Start of Season (SOS), DOY	*B. spiciformis*	*J. globiflora*	147	147	0.251085	146	0.802	1	ns
Start of Season (SOS), DOY	*B. spiciformis*	*P. tinctorius*	147	147	−1.25231	146	0.212	1	ns
Start of Season (SOS), DOY	*B. spiciformis*	Other	147	147	1.114212	146	0.267	1	ns
Start of Season (SOS), DOY	*J. globiflora*	*P. tinctorius*	147	147	−2.31359	146	0.022	0.133	ns
Start of Season (SOS), DOY	*J. globiflora*	Other	147	147	1.532201	146	0.128	0.768	ns
Start of Season (SOS), DOY	*P. tinctorius*	Other	147	147	3.934399	146	0.000129	0.000774	***
End of Season (EOS), DOY	*B. spiciformis*	*J. globiflora*	147	147	−5.0444	146	0.00000133	0.00000798	****
End of Season (EOS), DOY	*B. spiciformis*	*P. tinctorius*	147	147	−8.17748	146	1.29×10^{-13}	7.74×10^{-13}	****

Table 3. *Cont.*

Dependent Variable	Group1	Group2	n1	n2	Statistic	df	*p*	*p*.adj	*p*.adj.signif
End of Season (EOS), DOY	*B. spiciformis*	Other	147	147	−6.75319	146	3.19×10^{-10}	1.91×10^{-09}	****
End of Season (EOS), DOY	*J. globiflora*	*P. tinctorius*	147	147	−1.41649	146	0.159	0.954	ns
End of Season (EOS), DOY	*J. globiflora*	Other	147	147	−0.69654	146	0.487	1	ns
End of Season (EOS), DOY	*P. tinctorius*	Other	147	147	1.184922	146	0.238	1	ns
Length of Season (LOS), days	*B. spiciformis*	*J. globiflora*	147	147	−2.8078	146	0.006	0.034	*
Length of Season (LOS), days	*B. spiciformis*	*P. tinctorius*	147	147	−2.68929	146	0.008	0.048	*
Length of Season (LOS), days	*B. spiciformis*	Other	147	147	−3.86425	146	0.000167	0.001	**
Length of Season (LOS), Days	*J. globiflora*	*P. tinctorius*	147	147	0.48655	146	0.627	1	ns
Length of Season (LOS), days	*J. globiflora*	Other	147	147	−1.47262	146	0.143	0.858	ns
Length of Season (LOS), days	*P. tinctorius*	Other	147	147	−1.8983	146	0.06	0.358	ns
Base value	*B. spiciformis*	*J. globiflora*	147	147	8.718341	146	5.74×10^{-15}	3.44×10^{-14}	****
Base value	*B. spiciformis*	*P. tinctorius*	147	147	9.427326	146	8.96×10^{-17}	5.38×10^{-16}	****
Base value	*B. spiciformis*	Other	147	147	8.61576	146	1.04×10^{-14}	6.24×10^{-14}	****
Base value	*J. globiflora*	*P. tinctorius*	147	147	−0.33097	146	0.741	1	ns
Base value	*J. globiflora*	Other	147	147	−0.11164	146	0.911	1	ns
Base value	*P. tinctorius*	Other	147	147	0.277761	146	0.782	1	ns
Peak time	*B. spiciformis*	*J. globiflora*	147	147	2.176455	146	0.031	0.187	ns
Peak time	*B. spiciformis*	*P. tinctorius*	147	147	−0.07046	146	0.944	1	ns
Peak time	*B. spiciformis*	Other	147	147	5.43606	146	0.000000223	0.00000134	****
Peak time	*J. globiflora*	*P. tinctorius*	147	147	−2.07681	146	0.04	0.238	ns
Peak time	*J. globiflora*	Other	147	147	1.738827	146	0.084	0.505	ns
Peak time	*P. tinctorius*	Other	147	147	3.825538	146	0.000193	0.001	**
Peak value	*B. spiciformis*	*J. globiflora*	147	147	11.85848	146	3.84×10^{-23}	2.3×10^{-22}	****
Peak value	*B. spiciformis*	*P. tinctorius*	147	147	9.24546	146	2.62×10^{-16}	1.57×10^{-15}	****
Peak value	*B. spiciformis*	Other	147	147	15.60665	146	6.37×10^{-33}	3.82×10^{-32}	****
Peak value	*J. globiflora*	*P. tinctorius*	147	147	−4.60072	146	0.00000906	0.0000544	****
Peak value	*J. globiflora*	Other	147	147	5.515667	146	0.000000154	0.000000924	****
Peak value	*P. tinctorius*	Other	147	147	8.785372	146	3.89×10^{-15}	2.33×10^{-14}	****

[c] DOY = day of the year, a specific day within a calendar year; ns = non-significant (*p*-value $\geq$ 0.05); and "*", "**", "***", "****" indicate significant at *p*-value < 0.05, *p*-value < 0.01, *p*-value < 0.001 and *p*-value < 0.0001, respectively.

3.2. Modeling Between Phenological Metrics and Climatic Factors

To model phenological metrics with climate factors, the time-based metrics, SOS and EOS, were selected. For species, *B. spiciformis* and *J. globiflora* were chosen, with *J. globiflora* also representing *P. tinctorius* and other species.

3.2.1. Modeling Between SOS and Climatic Factors

The correlation analysis showed that skin temperature and solar radiation from the preceding month (September) and the month of SOS (October), as well as rainfall during the month of SOS (October), were highly correlated with the SOS of *B. spiciformis* (Figure 5). The same factors were also highly correlated with the SOS of *J. globiflora* (Figure 6). Except for skin temperature in October, which correlated positively with SOS, the other highly correlated factors showed a negative correlation.

Modeling variables with a correlation coefficient above 0.50 with SOS revealed that significant predictors for both *B. spiciformis* and *J. globiflora* were skin temperature and solar radiation from the month preceding the SOS (September). When these variables were combined in the models, their performance improved, as indicated by an increase in the adjusted R-squared and a decrease in Root Mean Square Error (RMSE) (Tables 4 and 5).
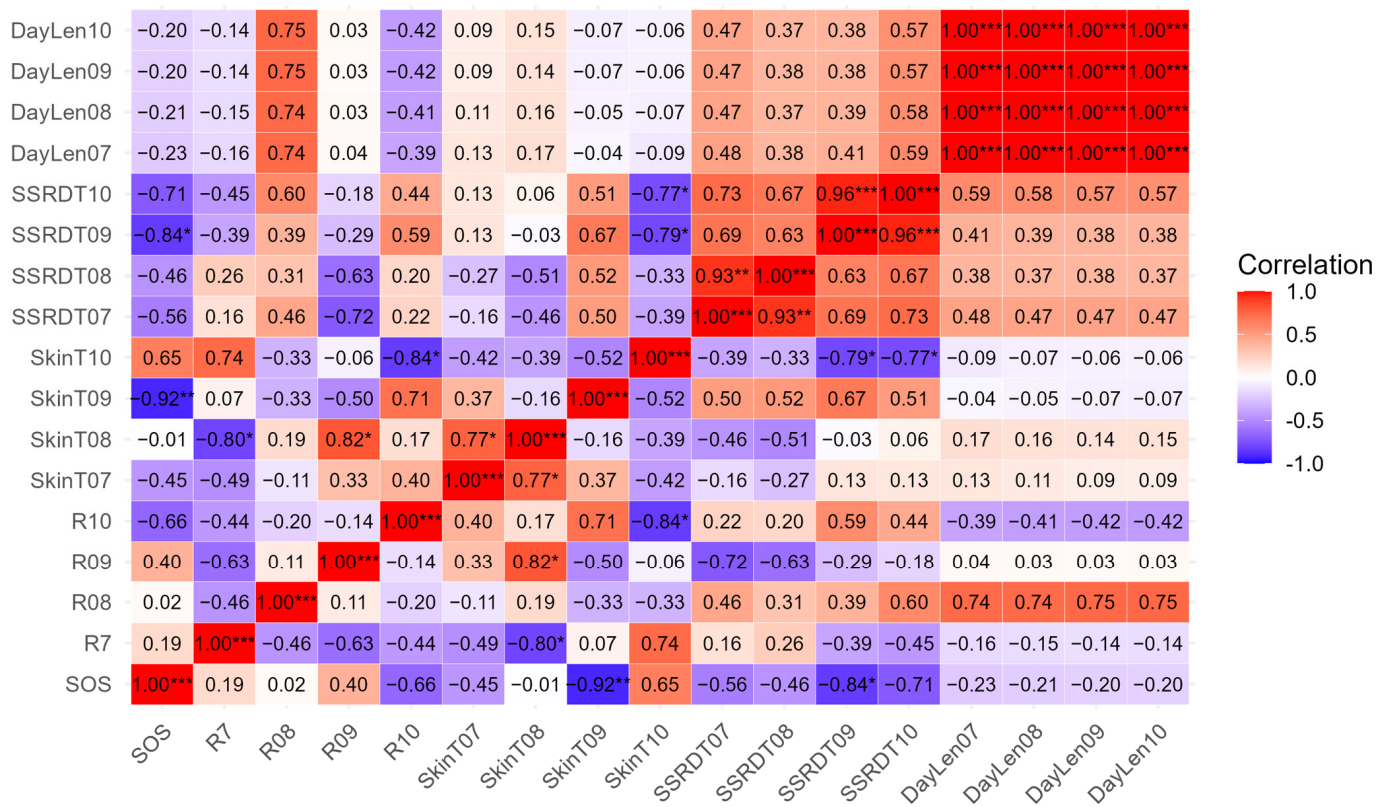
Figure 5. Correlation of seasonal and pre-season climatic factors with Start of Season (SOS) for *B. spiciformis.* R7 = rainfall July, R08 = rainfall August, R09 = rainfall September, R10 = rainfall October, SkinT07 = skin temperature July, SkinT08 = skin temperature August, SkinT09 = skin temperature September, SkinT10 = skin temperature October, SSRDT07 = surface solar radiation July, SSRDT08 = surface solar radiation August, SSRDT09 = surface solar radiation September, SSRDT10 = surface solar radiation October, DayLen07 = day length July, DayLen08 = day length August, DayLen09 = day length September, DayLen10 = day length October. Asterisks indicate significance levels: "*" for *p*-value < 0.05, "**"for *p*-value < 0.01, and "***" for *p*-value < 0.001.

Table 4. The effect of climatic factors on modeling the Start of Season (SOS) of *B. spiciformis* [d].

Variable	Adjusted R Squared	*p*-Value	Equations	RMSE	Significance
Skin temperature September (SkinT09)	0.8051	0.003841	SOS = 34835.2 − 117.3 SkinT09	20.68	***
Surface solar radiation September (SSRDT09)	0.6452	0.01821	SOS = 288.7 − 0.0000103SSRDT09	27.05	***
Surface solar radiation October (SSRDT10)	0.4131	0.07104			ns
Rainfall October (R10)	0.3293	0.1037			ns
Skin temperature October (SkinT10)	0.3028	0.116			ns
Surface solar radiation July (SSRDT07)	0.1712	0.1948			ns
Skin temperature September (SkinT09) + surface solar radiation September (SSRDT09)	0.8958	0.004827	SOS = 24500 − 82.1SkinT09 −0.00000504SSRDT09	13.47	***

[d] RMSE = Root Mean Square Error, SOS = Start of Season in day of the year, ns = non-significant (*p*-value ≥ 0.05); and "***" indicate significant *p*-value < 0.001.
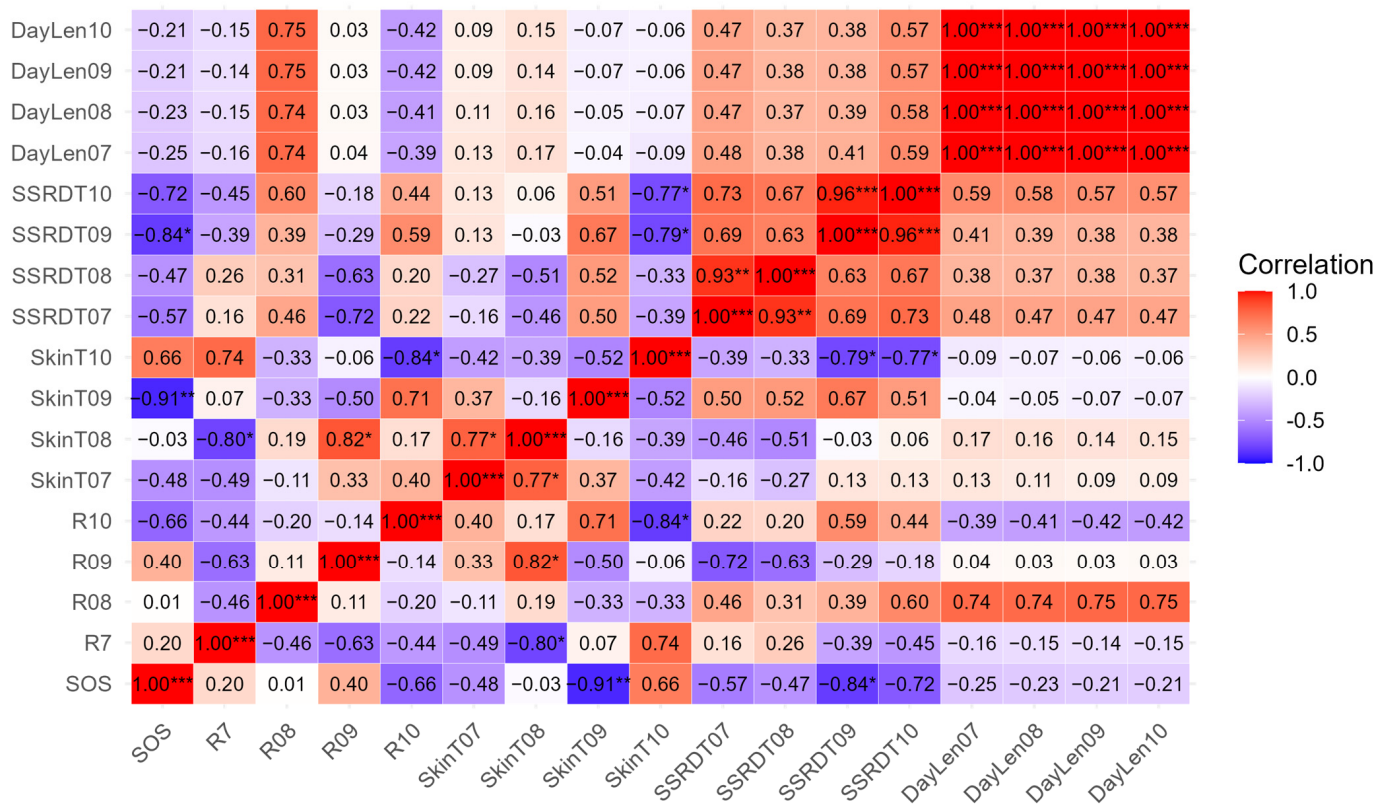
Figure 6. Correlation of seasonal and pre-season climatic factors with Start of Season (SOS) for *J. globiflora*. R7 = rainfall July, R08 = rainfall August, R09 = rainfall September, R10 = rainfall October, SkinT07 = skin temperature July, SkinT08 = skin temperature August, SkinT09 = skin temperature September, SkinT10 = skin temperature October, SSRDT07 = surface solar radiation July, SSRDT08 = surface solar radiation August, SSRDT09 = surface solar radiation September, SSRDT10 = surface solar radiation October, DayLen07 = day length July, DayLen08 = day length August, DayLen09 = day length September, DayLen10 = day length October. Asterisks indicate significance levels: "*" for *p*-value < 0.05, "**" for *p*-value < 0.01, and "***" for *p*-value < 0.001.

Table 5. The effect of climatic factors on modeling the Start of Season (SOS) of *J. globiflora* [e].

Variable	Adjusted R Squared	*p*-Value	Equations	RMSE	Significance
Skin temperature September (SkinT09)	0.7971	0.004262	SOS = 33922.79 − 114.24 SkinT09	19.99	***
Surface solar radiation September (SSRDT09)	0.6401	0.01891	SOS = 283.6 − 0.00001SSRDT09	26.52	***
Surface solar radiation October (SSRDT10)	0.4214	0.06828			ns
Rainfall October (R10)	0.3288	0.1039			ns
Skin temperature October (SkinT10)	0.3173	0.1092			ns
Surface solar radiation July (SSRDT07)	0.1871	0.1835			ns
Skin temperature September (SkinT09) + surface solar radiation September (SSRDT09)	0.8856	0.005813	SOS =23820 − 79.80SkinT09 − 0.000004925SSRDT09	13.57	***

[e] RMSE = Root Mean Square Error, SOS = Start of Season in day of the year; ns = non-significant (*p*-value ≥ 0.05); and "***" indicate significant at *p*-value < 0.001.

3.2.2. Modeling Between End of Season (EOS) and Climatic Factors

The correlation analysis revealed that factors highly correlated with the EOS of *B. spiciformis* (19 June) were surface solar radiation in May and June, skin temperature in May and June, and rainfall in June. These factors were negatively correlated with the EOS of *B. spiciformis* (Figure 7). In contrast, factors highly associated with the EOS of *J. globiflora* (3 July) included surface solar radiation in May, June, and July (the month of EOS), day length in July, skin temperature in May, June, and July, and rainfall in July. These factors also correlated negatively with the EOS of *J. globiflora* (Figure 8).
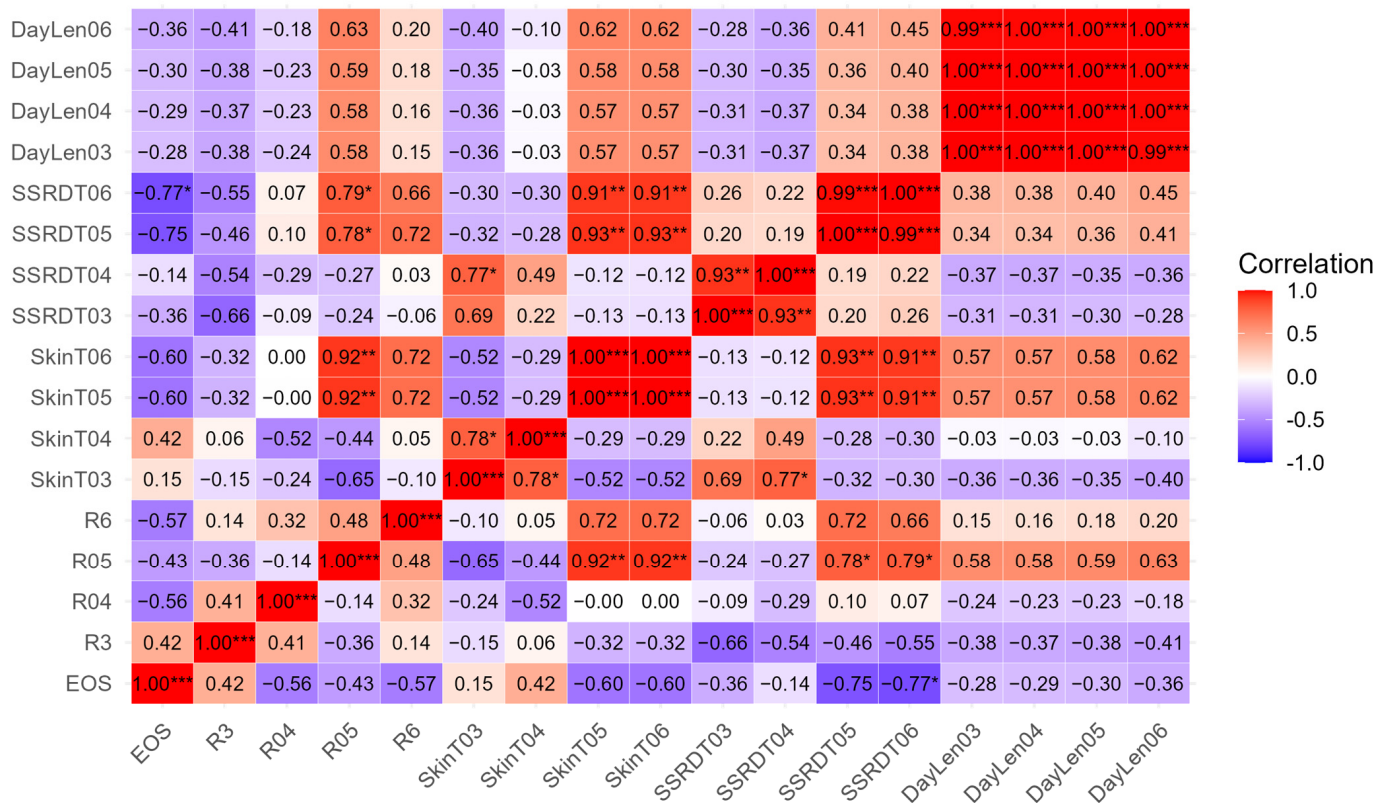

Figure 7. Correlation of seasonal and pre-season climatic factors with End of Season (EOS) for *B. spiciformis* R3 = rainfall March, R04 = rainfall April, R05= rainfall May, R6 = rainfall June, SkinT03 = skin temperature March, SkinT04 = skin temperature April, SkinT05 = skin temperature May, SkinT06 = skin temperature June, SSRDT03 = surface solar radiation March, SSRDT04 = surface solar radiation April, SSRDT05 = surface solar radiation May, SSRDT06 = surface solar radiation June, DayLen03 = day length March, DayLen04 = day length April, DayLen05 = day length May, DayLen06 = day length June. Asterisks indicate significance levels: "*" for *p*-value < 0.05, "**" for *p*-value < 0.01, and "***" for *p*-value < 0.001.

However, the linear model of highly correlated factors—with a correlation coefficient above 0.5—with the EOS of *B. spiciformis* and *J. globiflora* were modeled linearly, revealed that these factors were non-significant predictors (Tables 6 and 7). This non-significance was possibly due to a non-linear relationship between the factors and EOS, despite the high correlation. However, EOS was significantly modeled linearly from SOS, with an adjusted R-squared of 1 for both *B. spiciformis* and *J. globiflora* and a Root Mean Square Error (RMSE) of 3 and 2 for *B. spiciformis* and *J. globiflora*, respectively (Figure 9, Table 8).
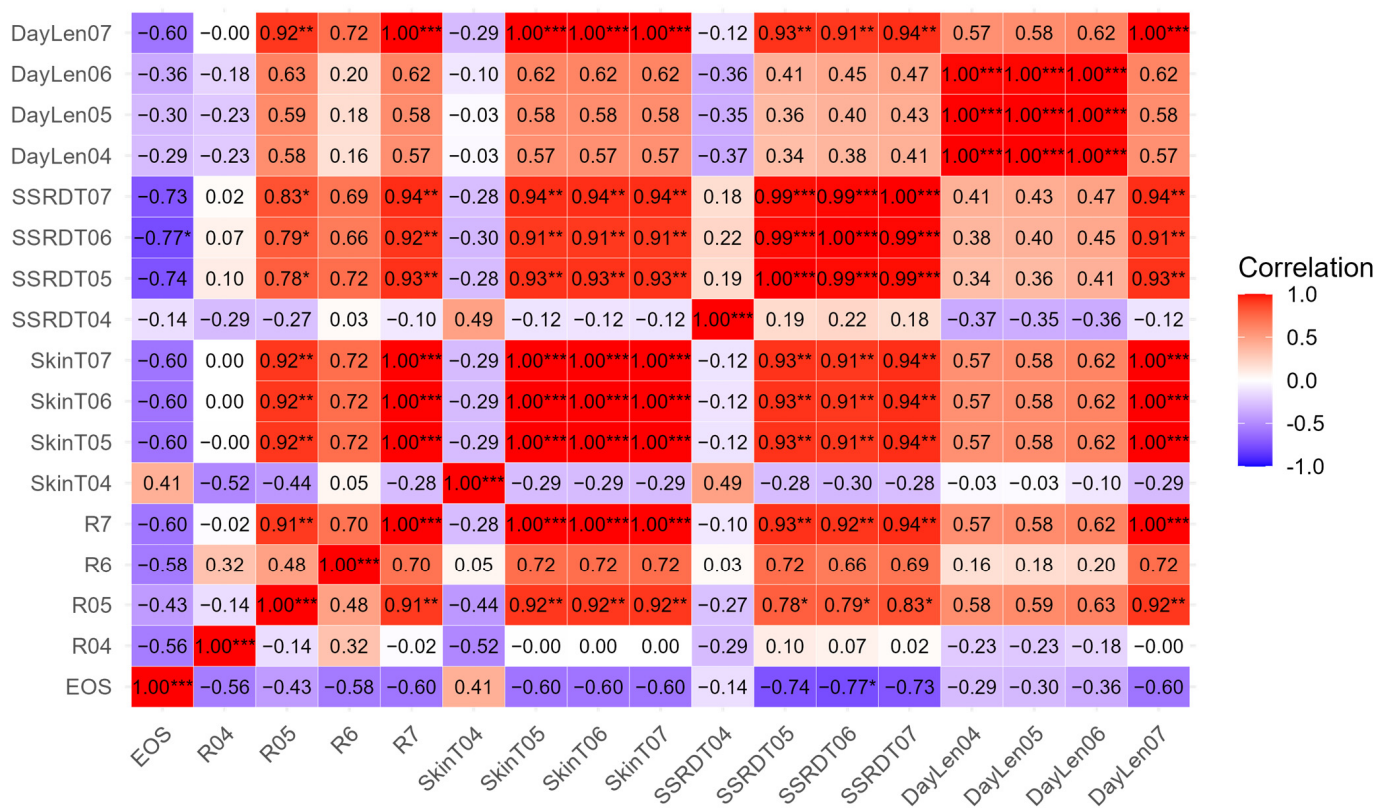
Figure 8. Correlation of seasonal and pre-season climatic factors with End of Season (EOS) for *J. globiflora.* R04= rainfall April, R05 = rainfall May, R6 = rainfall June, R7 = rainfall July, SkinT04 = skin temperature April, SkinT05 = skin temperature May, SkinT06 = skin temperature June, SkinT07 = skin temperature July, SSRDT04 = surface solar radiation April, SSRDT05 = surface solar radiation May, SSRDT06 = surface solar radiation June, SSRDT07 = surface solar radiation July, DayLen04 = day length April, DayLen05 = day length May, DayLen06 = day length June, DayLen07 = day length July. Asterisks indicate significance levels: "*" for *p*-value < 0.05, "**" for *p*-value < 0.01, and "***" for *p*-value < 0.001.

Table 6. The effect of climatic factors on modeling the End of Season (EOS) of *B. spiciformis* [f].

Variable	Adjusted R Squared	*p*-Value	Significance
Surface solar radiation June	0.3489	0.1275	ns
Surface solar radiation May	0.2444	0.181	ns
Skin temperature May	0.332	0.1353	ns
Skin temperature June	−0.05424	0.4374	ns
Rainfall June	−0.1758	0.6419	ns
Rainfall April	0.3674	0.1194	ns

[f] ns = non-significant (*p*-value ≥ 0.05).

Table 7. The effect of climatic factors on modeling the End of Season (EOS) of *J. globiflora* [g].

Variable	Adjusted R Squared	*p*-Value	Significance
Surface solar radiation June	0.3407	0.1313	ns
Surface solar radiation May	0.2414	0.1827	ns
Surface solar radiation July	0.2197	0.1957	ns
Day length July	−0.2354	0.8387	ns
Skin temperature July	−0.2493	0.9644	ns
Skin temperature June	−0.06411	0.4502	ns

Table 7. *Cont.*

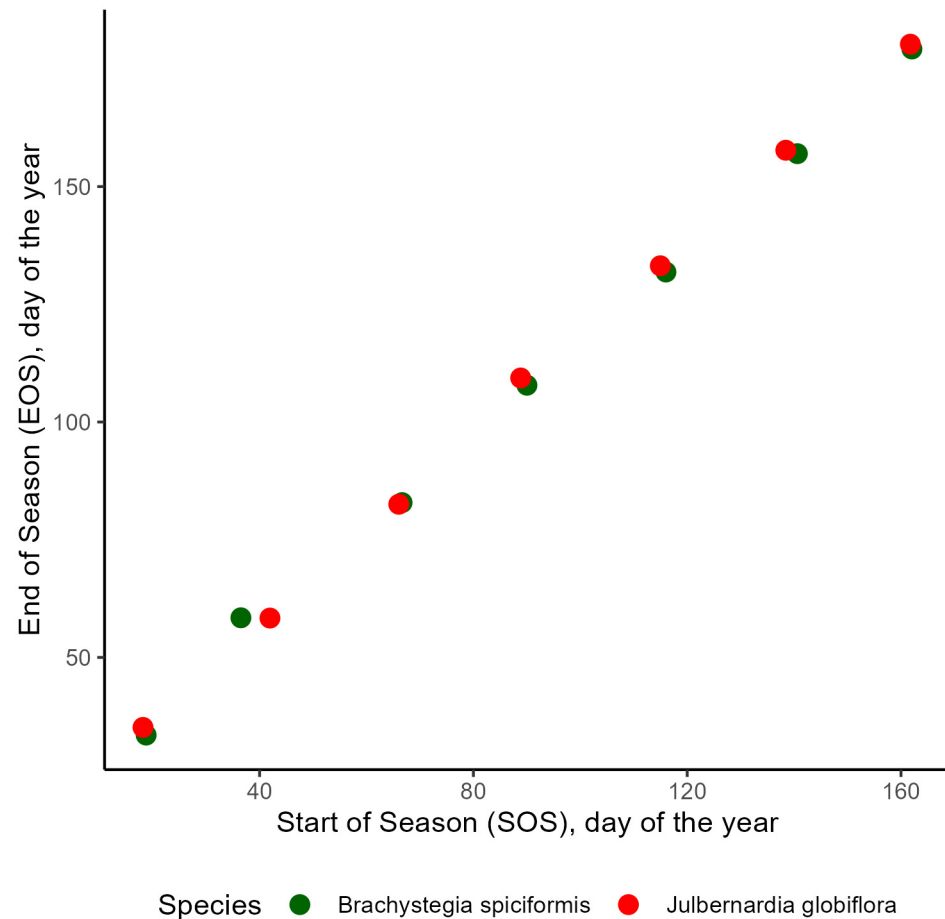| Variable	Adjusted R Squared	*p*-Value	Significance
Rainfall July	−0.244	0.8966	ns
Skin temperature May	0.3127	0.1446	ns
Rainfall June	−0.1653	0.6184	ns
Rainfall April	0.3734	0.1168	ns

[g] ns = non-significant (*p*-value ≥ 0.05).

Figure 9. Correlation between Start of Season and End of Season for *B. spiciformis* and *J. globiflora* across seasons.

Table 8. The effect of Start of Season (SOS) on modeling the End of Season (EOS) of *B. spiciformis* and *J. globiflora* [h].

Variable	*r*	Adjusted R Squared	*p*-Value	Equations	RMSE	Significance	Species
SOS	0.999	0.9978	<0.001	EOS = 17.85 + 0.99SOS	3.01	***	*B. spiciformis*
SOS	0.9997	0.9994	<0.001	EOS = 16.45 + 1.02SOS	2.30	***	*J. globiflora*

[h] RMSE = Root Mean Square Error, SOS = Start of Season, EOS = End of Season. An asterisk "***" indicates a significance level of $p < 0.001$.

4. Discussion

There were no significant differences in the Start of Season (SOS) among the dominant tree species in early October. This finding on the timing of SOS for the dominant miombo tree species aligns with those of [32], who found that the SOS of woody savannas and savanna mosaics in Eastern Africa occurs from late August to early November.

The SOS of these tree species in early October is significantly correlated with skin temperature and surface solar radiation from September, the preceding month (Figures 5 and 6). Higher values of surface solar radiation and skin temperature are associated with an earlier SOS, while lower values correspond to a later SOS. Surface solar radiation refers to the amount of solar energy reaching the Earth's surface, while skin temperature indicates the temperature of the Earth's surface.

Surface solar radiation and skin temperature are positively related. In September, surface solar radiation and skin temperature reach their highest values (Figure 8), implying that increased solar energy leads to warmer temperatures. These conditions trigger growth in miombo tree species. Warmer temperature cues plant development, while sunlight is crucial for initiating photosynthetic activities. This period is particularly favorable for photosynthesis, as it also marks the onset of the wet season (Figure 10B).
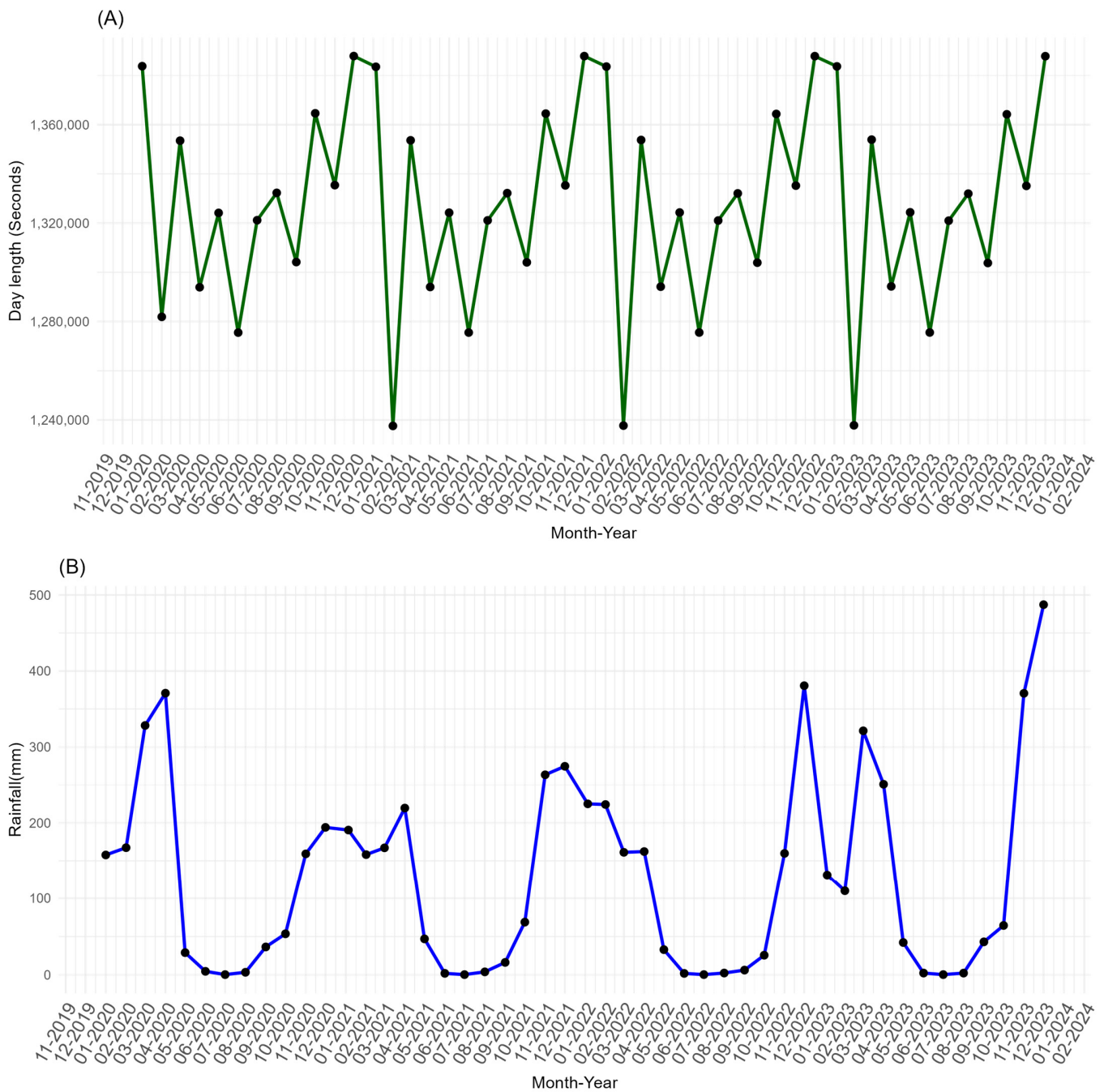

Figure 10. Monthly trends of (**A**) day length, and (**B**) rainfall from January 2020 to December 2023.

Moreover, the skin temperature and surface solar radiation in September were the most significant predictors for modeling the SOS of miombo tree species, specifically *B. spiciformis* and *J. globiflora*. Skin temperature and surface solar radiation individually explained 81% and 65% of the variance in the SOS of *B. spiciformis*, respectively. When both variables were included in the model, they collectively explained 90% of the variance in the SOS of *B. spiciformis*. For *J. globiflora*, skin temperature and surface solar radiation in September individually explained 80% and 64% of the variance in the SOS. When both variables were included, they explained 89% of the variance in the SOS of *J. globiflora*.

However, there were significant differences in the day of year for the end of season (EOS) among the dominant tree species, contributing to variations in the length of season (LOS) between *B. spiciformis* and the other species. The EOS for *B. spiciformis* occurred on June 19, while those for *J. globiflora*, *P. tinctorius*, and others ranged from July 3 to 6. These EOS dates for the tree species are earlier than the EOS for woody savanna/savanna mosaic, which [32] found to occur from mid-July to late August in Eastern Africa. These differences may be due to spatial factors, as we studied phenology metrics at the tree species level for a representative site in western Tanzania, while [32] examined phenology metrics for woody savanna/savanna mosaics across Eastern Africa. The high variation in vegetation cover and species within woody savanna/savanna mosaics, along with diverse climate conditions across Eastern Africa, likely influences EOS timing.

The End of Season (EOS) for *B. spiciformis* on 19 June 19 is significantly correlated with surface solar radiation in June (Figure 7). Similarly, the EOS for *J. globiflora* on 3 July is significantly correlated with surface solar radiation in June (Figure 8). Surface solar radiation is negatively correlated with EOS, indicating that higher surface solar radiation values are associated with an earlier EOS, while lower values correspond to a later EOS. During the EOS period in June and early July, surface solar radiation at the site begins to increase (Figure 11A), contributing to a rise in skin temperature (Figure 11B). Additionally, this period marks the onset of the dry season (Figure 10B). Although surface solar radiation influences the EOS, it demonstrated a non-linear relationship when used in models to estimate EOS.

SOS was the most significant linear predictor for EOS, explaining 100% of the variance in EOS. SOS and EOS were positively related, indicating that a delay in SOS results in a later EOS, while an earlier SOS leads to an earlier EOS. This relationship between SOS and EOS reflects a shift in the growth cycle due to seasonal variability, which may contribute to significant differences in phenology metrics between seasons.

Thus, surface solar radiation is the most significant factor explaining variation in the phenology of dominant miombo tree species. However, this contrasts with [19], who reported that the Start of Season (SOS) in woodlands is controlled by the photoperiod. This difference may also be due to spatial scale, as [19] analyzed the relationship between climatic drivers and the phenology of woodlands, combining woody savanna, savanna mosaic, and mixed forest across the African continent from the MCD12Q1 data. MCD12Q1 is an annual global land cover data product with a 500-meter spatial resolution, produced by NASA's Moderate Resolution Imaging Spectroradiometer (MODIS) on the Terra and Aqua satellites. In contrast, this study focused on tree species phenology at the crown level at a representative site in western Tanzania. Therefore, studying phenology at a finer scale—specifically at sites with similar climates and focused on individual tree species—is essential for obtaining clear insights that could help assess the impact of climate variability and change on African ecosystems.

Despite the valuable insights obtained, this study was limited to eight years—seven miombo seasons—offering a snapshot of tree species' responses to climate variables and their variability. Additionally, while the results aligned with field observations, there was insufficient ground phenology data for thorough comparison. This study also focused on a small, representative site of miombo woodland in western Tanzania, which does not capture the full range of environmental conditions across miombo woodlands in Tanzania and Southern Africa. Nevertheless, the findings suggest that the phenology of miombo tree

species can be effectively monitored through remote sensing. Furthermore, the association of miombo woodland species with surface solar radiation and skin temperature highlights their potential vulnerability to shifts in climate patterns.
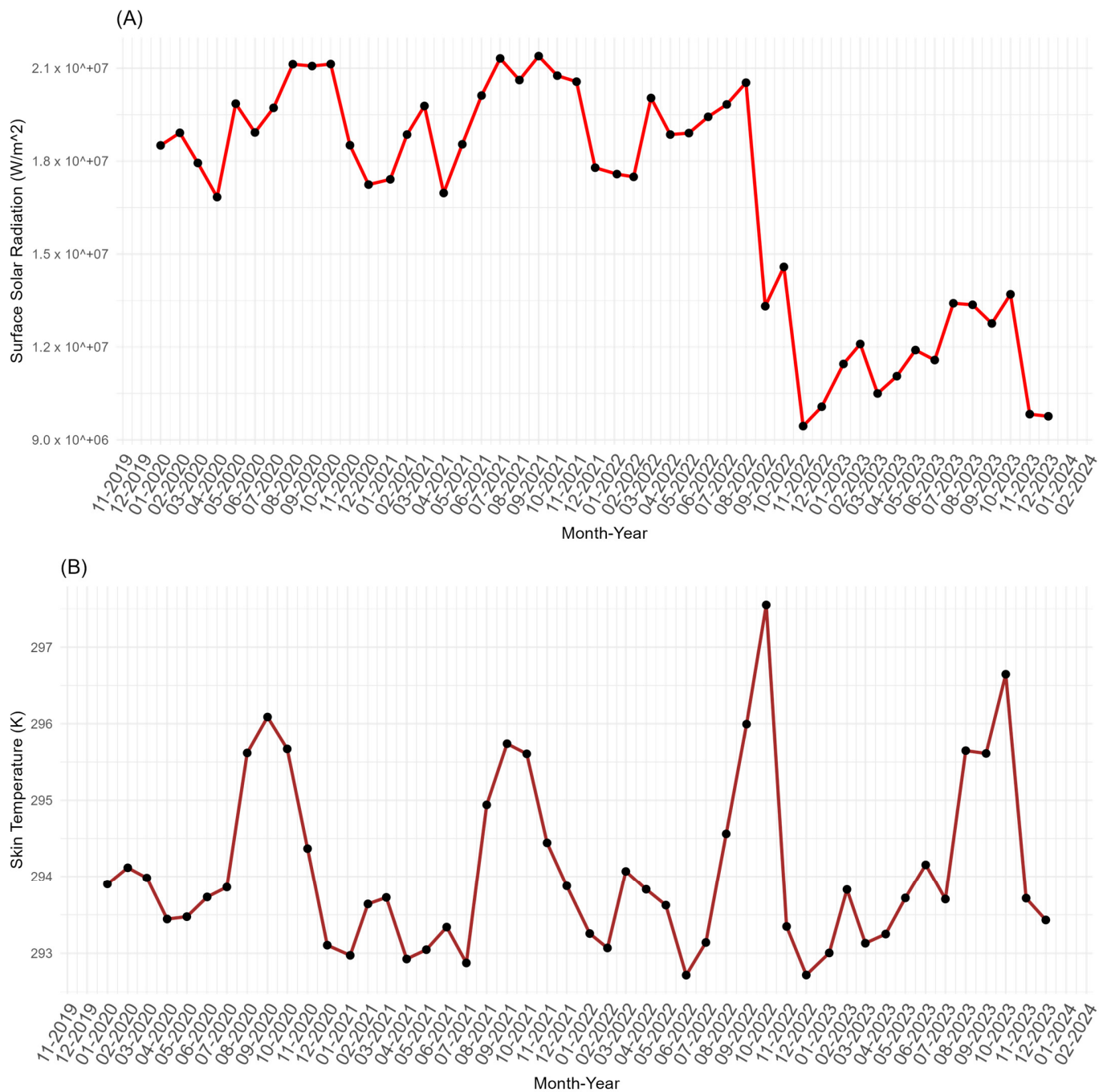
(A)

(B)

Figure 11. Monthly trends in (**A**) surface solar radiation and (**B**) skin temperature from January 2020 to December 2023.

5. Conclusions

The EOS, LOS, base value, and peak value of *B. spiciformis* differ from those of other species. Additionally, surface solar radiation and skin temperature are significant predictors of the SOS for miombo tree species, while SOS itself serves as an important predictor of EOS. These findings enhance our understanding of how miombo tree species respond to climatic factors, with solar radiation and skin temperature playing key roles in influencing their phenology. This information can be valuable for predicting shifts in tree species

phenology under the current climate change trends and could inform further research on monitoring the phenology of miombo species. Future studies should expand the dataset to include more seasons to better understand the effects of climate change on the phenology of miombo tree species. Moreover, future research should cover a broader area of miombo woodlands, incorporating diverse elevations and soil conditions, for more comprehensive modeling of tree species' phenological responses to climate. Additionally, establishing networks for ground phenology monitoring will be essential to validate Land Surface Phenology (LSP).
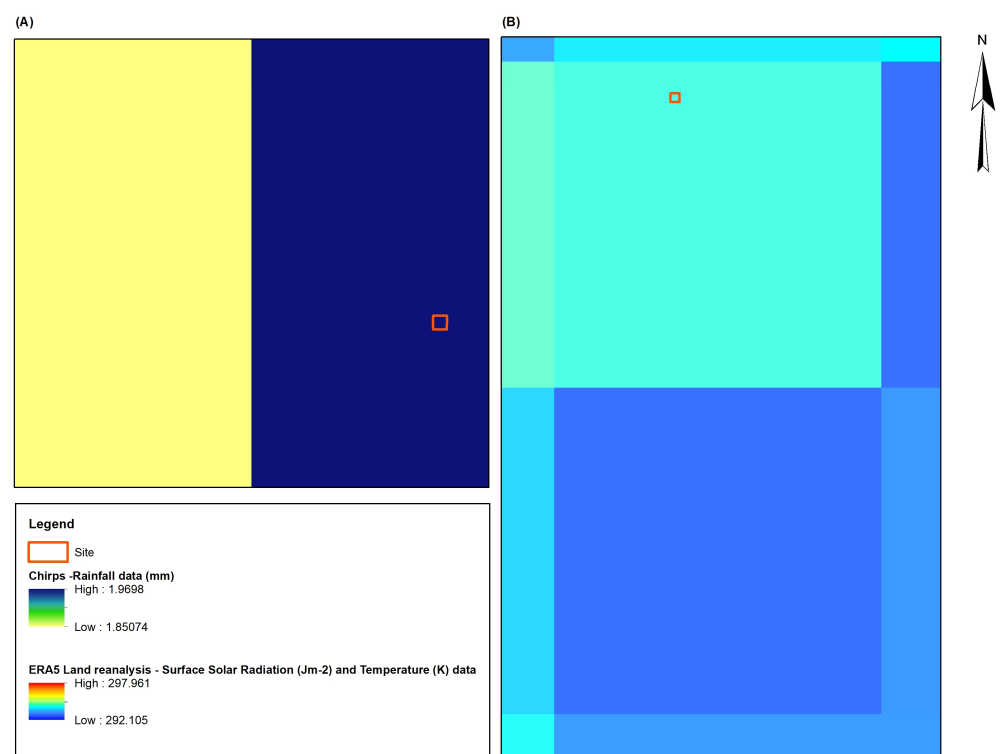
Appendix A

Figure A1. Overlay of the site on (**A**) CHIRPS rainfall data, and (**B**) ERA-5 Land reanalysis surface solar radiation and temperature data.

Appendix B

Table A1. Dates and cloud cover (%) of acquired PlanetScope images.

Years	2017		2018		2019		2020		2021		2022		2023		2024	
Month	Date	Cloud Cover (%)	Date	Cloud Cover (%)	Date	Cloud Cover (%)	Date	Cloud Cover (%)	Date	Cloud Cover (%)	Date	Cloud Cover (%)	Date	Cloud Cover (%)	Date	Cloud Cover (%)
January	05	100	03	15	04	0	11	90	01	77	02	100	03	0	07	0
January	24	3	27	0	26	0	17	0	24	33	31	0	23	0	18	0
February	13	0	13	0	12	0	13	34	03	9	08	100	01	6	07	33
February	14	1	18	0	25	52	22	11	14	31	25	40	17	0	20	0
March	14	85	05	23	04	37	08	100	02	0	01	0	09	100	07	0
March	31	0	22	0	22	0	29	17	19	28	19	0	28	0	16	12
April	04	4	16	0	08	0	06	47	12	49	04	12	03	25	09	0
April	30	0	30	9	19	0	15	0	20	89	10	0	19	0	18	16
May	04	0	10	13	05	2	04	14	12	60	04	0	07	14	02	0
May	21	0	24	0	18	71	26	0	26	0	18	0	19	0	19	0
June	09	0	04	0	05	0	04	0	01	0	02	0	07	0	01	0
June	19	0	24	0	18	0	25	0	23	0	19	0	19	0	21	0
July	02	0	03	0	02	0	02	0	10	0	01	0	03	0	01	0
July	21	1	20	0	19	0	26	0	24	0	23	0	17	0	18	0
August	04	0	05	0	04	0	01	0	02	0	06	0	06	0	06	0
August	21	0	16	0	20	0	23	0	21	0	24	0	17	0	17	0
September	09	0	02	0	05	0	03	0	05	0	02	0	02	0	02	0
September	22	0	24	0	23	0	21	0	19	0	24	0	15	0	15	0
October	06	0	06	0	05	0	03	0	09	0	05	0	02	0	02	0
October	22	0	22	0	27	0	23	0	21	0	24	0	20	0	20	0
November	01	0	05	0	07	0	02	0	5	62	05	0	01	0	01	0
November	18	5	27	0	16	0	17	100	24	0	21	100	21	100	21	100
December	07	15	06	100	12	75	05	46	07	0	07	0	02	0	02	0
December	21	2	25	10	24	0	22	99	27	0	16	0	29	100	29	100

References

1. Frost, P. The Ecology of Miombo Woodlands. In *The Miombo in Transition: Woodlands and Welfare in Africa*; Campbell, B., Ed.; Center for International Forestry Research (CIFOR): Bogor, Indonesia, 1996; pp. 11–57. ISBN 9798764072.
2. FAO Africa: Ecological Zones. In *Global Forest Resources Assessment 2000: Main Report*; FAO: Rome, Italy, 2001; FAO Forestry Paper 140; pp. 103–107.
3. *Global Ecological Zones for FAO Forest Reporting: 2010 Update*; FAO: Rome, Italy, 2012; Volume 179, p. 42.
4. Dziba, L.; Ramoelo, A.; Ryan, C.; Harrison, S.; Pritchard, R.; Tripathi, H.; Sitas, N.; Selomane, O.; Engelbrecht, F.; Pereira, L.; et al. *Scenarios for Just and Sustainable Futures in the Miombo Woodlands*; Ribeiro, N., Katerere, Y., Chirwa, P., Grundy, I., Eds.; Miombo Woo.; Springer: Cham, Switzerland, 2020; ISBN 9783030501037.
5. Abdallah, J.; Monela, G. Overview of Miombo Woodlands in Tanzania. In Proceedings of the First MITMIOMBO Project Workshop, Morogoro, Tanzania, 6–12 February 2007; Working Papers of the Finnish Forest Research Institute 50. METLA: Helsinki, Finland, 2007; pp. 9–23.
6. Dewees, P.; Campbell, B.; Katerere, Y.; Sitoe, A.; Cunningham, A.; Angelsen, A.; Wunder, S. *Managing the Miombo Woodlands of Southern Africa: Policies, Incentives, and Options for the Rural Poor*; Program on Forests (PROFOR): Washington, DC, USA, 2011.
7. Lusambo, L.P. Economics on the Household Energy in Miombo Woodlands of Eastern and Southern Tanzania. Ph.D. Thesis, University of Bangor, Gwynedd, UK, 2009.
8. Syampungani, S.; Chirwa, P.W.; Akinnifesi, F.K.; Sileshi, G.; Ajayi, O.C. The Miombo Woodlands at the Cross Roads: Potential Threats, Sustainable Livelihoods, Policy Gaps and Challenges. *Nat. Resour. Forum* **2009**, *33*, 150–159. [CrossRef]
9. *URT National Forest Resources Monitoring and Assessment of Tanzania Mainland: Main Results*; Ministry of Natural Resources and Tourism: Dar Es Salaam, Tanzania, 2015.
10. Corbera, E.; Estrada, M.; Brown, K. Reducing Greenhouse Gas Emissions from Deforestation and Forest Degradation in Developing Countries: Revisiting the Assumptions. *Clim. Change* **2010**, *100*, 355–388. [CrossRef]
11. John, E.; Bunting, P.; Hardy, A.; Roberts, O.; Giliba, R.; Silayo, D.S. Modelling the Impact of Climate Change on Tanzanian Forests. *Divers. Distrib.* **2020**, *26*, 1663–1686. [CrossRef]
12. Jinga, P.; Palagi, J. Dry and Wet Miombo Woodlands of South-Central Africa Respond Differently to Climate Change. *Environ. Monit. Assess.* **2020**, *192*, 372. [CrossRef] [PubMed]
13. Cleland, E.E.; Chuine, I.; Menzel, A.; Mooney, H.A.; Schwartz, M.D. Shifting Plant Phenology in Response to Global Change. *Trends Ecol. Evol.* **2007**, *22*, 357–365. [CrossRef] [PubMed]
14. van Vliet, A.J.H.; Schwatz, M.D. Phenology and Climate: The Timing of Life Cycle Events as Indicators of Climatic Variability and Change. *Int. J. Climatol.* **2002**, *22*, 1713–1714. [CrossRef]
15. Gray, R.E.J.; Ewers, R.M. Monitoring Forest Phenology in a Changing World. *Forests* **2021**, *12*, 297. [CrossRef]
16. Pereira, H.M.; Ferrier, S.; Walters, M.; Geller, G.N.; Jongman, R.H.G.; Scholes, R.J.; Bruford, M.W.; Brummitt, N.; Butchart, S.H.M.; Cardoso, A.C.; et al. Essential Biodiversity Variables. *Science* **2013**, *339*, 277–278. [CrossRef] [PubMed]
17. Adole, T.; Dash, J.; Atkinson, P. A Systematic Review of Vegetation Phenology in Africa. *Ecol. Inform.* **2016**, *34*, 117–128. [CrossRef]
18. Chidumayo, E.N. Climate and Phenology of Savanna Vegetation in Southern Africa. *J. Veg. Sci.* **2001**, *12*, 347. [CrossRef]
19. Adole, T.; Dash, J.; Rodriguez-Galiano, V.; Atkinson, P.M. Photoperiod Controls Vegetation Phenology across Africa. *Commun. Biol.* **2019**, *2*, 1–16. [CrossRef] [PubMed]
20. Adole, T.; Dash, J.; Atkinson, P. Large Scale Pre-Rain Vegetation Green up across Africa. *Glob. Chang. Biol.* **2018**, *24*, 4054–4068. [CrossRef] [PubMed]
21. Guan, K.; Wood, E.F.; Medvigy, D.; Kimball, J.; Pan, M.; Caylor, K.K.; Sheffield, J.; Xu, X.; Jones, M.O. Phenology of African Savannas and Woodlands. *J. Geophys. Res. Biogeosciences* **2014**, *119*, 1652–1669. [CrossRef]
22. Pereira, H.M.; Belnap, J.; Monika, B.; Brummitt, N.; Garcia-moreno, J.; Gregory, R.; Martin, L.; Peng, C.; Schmeller, D.; van Swaay, C. Monitoring Essential Biodiversity Variables at the Species Level. In *The GEO Handbook on Biodiversity Observation Networks*; Walters, M., Scholes, R., Eds.; Springer: Cham, Switzerland, 2017; pp. 79–105. [CrossRef]
23. *MARI Soils of Tanzania and Their Potential for Agriculture Development*; Mlingano Agricultural Research Institute, Department of Research and Training, Ministry of Agriculture, Food Security and Co-Operatives: Tanga, Tanzania, 2006.
24. Grime, J. Benefits of Plant Diversity to Ecosystems: Immediate, Filter and Founder Effects. *J. Ecol.* **1998**, *86*, 902–910. [CrossRef]
25. Vrieling, A.; De Leeuw, J.; Said, M.Y. Length of Growing Period over Africa: Variability and Trends from 30 Years of NDVI Time Series. *Remote Sens.* **2013**, *5*, 982–1000. [CrossRef]
26. CHIRPS: Rainfall Estimates from Rain Gauge and Satellite Observations | Climate Hazards Center—UC Santa Barbara. Available online: https://www.chc.ucsb.edu/data/chirps (accessed on 17 July 2024).
27. Munoz Sabater, J. ERA5-Land Monthly Averaged Data from 1950 to Present. Copernicus Climate Change Service (C3S) Climate Data Store (CDS). Available online: https://cds.climate.copernicus.eu/datasets/reanalysis-era5-land-monthly-means?tab=overview (accessed on 3 November 2024).
28. Sunrise and Sunset Times in 5°27′40.9″S, 30°29′12.9″E. Available online: https://www.timeanddate.com/sun/@-5.46138,30.48694 (accessed on 15 July 2024).
29. Eklundh, L.; Jöhnsson, P. *TIMESAT 3.3 Software Manual, Version 3.3*; Lund Universitet: Lund, Sweden, 2017.
30. Jönsson, P.; Eklundh, L. TIMESAT—A Program for Analyzing Time-Series of Satellite Sensor Data. *Comput. Geosci.* **2004**, *30*, 833–845. [CrossRef]

31.   Jönsson, P.; Eklundh, L. Seasonality Extraction by Function Fitting to Time-Series of Satellite Sensor Data. *IEEE Trans. Geosci. Remote Sens.* **2002**, *40*, 1824–1832. [CrossRef]

32.   Adole, T.; Dash, J.; Atkinson, P.M. Characterising the Land Surface Phenology of Africa Using 500 m MODIS EVI. *Appl. Geogr.* **2018**, *90*, 187–199. [CrossRef]